$\mathbb{T}$ Operator Bounds on Angle-Integrated Absorption and Thermal Radiation for Arbitrary Objects

Sean Molesky,[1] Weiliang Jin,[2] Prashanth S. Venkataram,[1] and Alejandro W. Rodriguez[1,*]
[1]Department of Electrical Engineering, Princeton University, Princeton, New Jersey 08544, USA
[2]Department of Electrical Engineering, Standford University, Stanford, California 94305, USA

(Received 11 July 2019; published 20 December 2019)

We derive fundamental per-channel bounds on angle-integrated absorption and thermal radiation for arbitrarily structured bodies—for any given material susceptibility and bounding region—that simultaneously encode both the per-volume limit on polarization set by passivity and geometric constraints on radiative efficiencies set by finite object sizes through the scattering $\mathbb{T}$ operator. We then analyze these bounds in two practical settings, comparing against prior limits as well as near optimal structures discovered through topology optimization. Principally, we show that the bounds properly capture the physically observed transition from the volume scaling of absorptivity seen in deeply subwavelength objects (nanoparticle radius or thin film thickness) to the area scaling of absorptivity seen in ray optics (blackbody limits).

DOI: 10.1103/PhysRevLett.123.257401

Motivated by the increasing control of light offered by micro- and nanoscale structuring [1,2], impetus to find bounds analogous to the blackbody limit for geometries that violate the assumptions of ray optics (nanoparticles [3], thin films [4], photonic crystals [5,6], etc.) has steadily grown over the past few decades. It is now well established that the absorption (radiative thermal emission) cross sections of a compact object can be much greater than its geometric area [7–12] ("super-Planckian" emission), and that deeply subwavelength films can achieve near unity absorptivity via surface texturing [13,14]. Limits applicable to all length scales and materials could both provide insight into these representative phenomena and guide efforts in related application areas such as integrated and metaoptics [15–17], photovoltaics [18–21], and photon sources [22–24].

Development of bounds for arbitrary objects has primarily followed two overarching strategies: modal decompositions based on quasinormal, Fourier, and/or multipole expansions [25–33], relating absorption cross section to the number of excitable optical modes (channels), or material bounds, utilizing energy [34,35] and/or spectral sum rules [36–42] to constrain achievable polarization response. Separately, each of these approaches present challenges for photonic design. Modal decompositions incorporate the specific size and shape characteristics of a body through expansion coefficients, and hence, inherently, require some enumeration and characterization of the participating modes to determine the range of values these coefficients can take [26,39,40]. Although fundamental considerations (transparency, energy, size, etc.) can and have been used in this regard [28,33,41,43], such cutoffs have yet to tightly bound potential coefficient values for arbitrary compact geometries, particularly when applied to metallic nanoparticles and antennas [27,35,44]. Conversely, material bounds set by intrinsic dissipation naturally reproduce the volumetric scaling of absorptivity characteristic of deeply subwavelength objects (and are highly accurate for the special case of weak polarizability in this regime [35]). However, because such approaches intrinsically suppose an optimally large response field existing at all points within an arbitrary object for any incident field, the same volumetric scaling persists for all length scales. Consequently, material bounds rapidly become too loose beyond quasistatic settings, yielding unphysical divergences with both increasing object size and material response.

In this Letter, we derive bounds on thermal radiation and absorption that combine these two approaches, linking the impact of material response with the influence of an object's geometry through the scattering $\mathbb{T}$ operator. This leads to a per-channel limit on integrated absorption capturing both material and radiative losses through the singular values of the imaginary part of the vacuum Green function. The result is applicable to objects of any size, exhibiting a smooth transition in absorptivity from the volume scaling achievable in the quasistatic (deeply subwavelength) regime to the area scaling limit of macroscopic ray optics. Further, the bounds always asymptotically approach the ray optics limit when all characteristic lengths are large and diverge sublogarithmically (rather than linearly) with material quality for objects of finite extent, significantly reducing cross-section limits for typical optical media even when all characteristic lengths are small. Throughout, we compare the present results to prior bounds as well as structures discovered using topology optimization, realizing a variety of examples (metallic and dielectric) that nearly achieve the predicted limits.

Derivation.—From the relations of scattering theory, both the power scattered from an incident field ($|\mathbf{E}_{\text{inc}}\rangle$)

and the thermal radiation emitted at a temperature T can be expressed in terms of the scattering $\mathbb{T}$ operator of an object and the vacuum Green function $\mathbb{G}^{\text{vac}}$ [45] as

$$P_{\text{sct}}(\omega) = \frac{k_o}{2Z}\langle \mathbf{E}_{\text{inc}}|\mathbb{T}^\dagger \text{Im}[\mathbb{G}^{\text{vac}}]\mathbb{T}|\mathbf{E}_{\text{inc}}\rangle = \frac{k_o}{2Z}\langle \mathbf{E}_{\text{inc}}|\text{Im}[\mathbb{T}] - \mathbb{T}^\dagger \text{Im}[\mathbb{V}^{-1^\dagger}]\mathbb{T}|\mathbf{E}_{\text{inc}}\rangle \quad (1)$$

and

$$H(\omega, T) = \Pi(\omega, T)\Phi(\omega), \qquad \Phi = \frac{2}{\pi}\text{Tr}\{\text{Im}[\mathbb{G}^{\text{vac}}](\text{Im}[\mathbb{T}] - \mathbb{T}^\dagger \text{Im}[\mathbb{G}^{\text{vac}}]\mathbb{T})\}. \quad (2)$$

Here, ω is the angular frequency, $k_o = 2\pi/\lambda$ is the wave number, Z is the impedance of free space, $\Pi(\omega) = \hbar\omega/[\exp(\beta\hbar\omega) - 1]$ with $(\beta = 1/k_B T)$ is the Planck energy of a harmonic oscillator, $\text{Tr}[\cdots]$ denotes the trace, $\text{Im}[\mathbb{T}] = (\mathbb{T} - \mathbb{T}^*)/2i$, and, by Kirchhoff's law of thermal radiation, Φ is the object's angle-integrated absorption [46]. (A synopsis of scattering formalism, along with a derivation of Eq. (2), is provided in Supplemental Material [47] .) For a passive object, scattered power must be positive for any incident field. As such, Eq. (1) simultaneously dictates that all singular values of the $\mathbb{T}$ operator must be smaller than the material figure of merit ζ,

$$\|\mathbb{T}\| \leq \zeta = \frac{|\chi(\omega)|^2}{\text{Im}[\chi(\omega)]}, \quad (3)$$

which was similarly derived in Ref. [35] for polarization fields, and that $\text{Im}[\mathbb{T}]$ is positive definite.

As $\text{Im}[\mathbb{G}^{\text{vac}}]$ is real-symmetric positive definite, it can be expressed via a singular value decomposition as

$$\text{Im}[\mathbb{G}^{\text{vac}}] = \sum_i \rho_i |\mathbf{q}_i\rangle\langle\mathbf{q}_i|, \quad (4)$$

where, as supported by our later analysis, each ρ_i (eigenvalue) can be equated to the outgoing radiative flux of the ith mode—the ith *radiative efficacy* of the domain. The set $\{\rho_i\}$ plays an analogous role to the coupling coefficients $\{g_{ij}\}$ used by Miller in setting limits on far-field optical communication [41]. Consider Eq. (2) using this expansion, $\Phi = (2/\pi)\sum_i \rho_i \text{Im}[\langle\mathbf{q}_i|\mathbb{T}|\mathbf{q}_i\rangle] - \rho_i^2|\langle\mathbf{q}_i|\mathbb{T}|\mathbf{q}_i\rangle|^2 - (2/\pi)\sum_{\{(i,j)|i\neq j\}} \rho_i\rho_j|\langle\mathbf{q}_i|\mathbb{T}|\mathbf{q}_j\rangle|^2$. Now, take $\mathbb{T}_{\text{opt}}$ to be a general operator described by the properties $(\mathbb{T}_{\text{opt}})^T = \mathbb{T}_{\text{opt}}$ (reciprocity), $\|\mathbb{T}_{\text{opt}}\| \leq \zeta$ (passivity), and $\text{Im}[\mathbb{T}_{\text{opt}}]$ positive definite (passivity), ignoring all other physical constraints that any true $\mathbb{T}$ operator must satisfy. In this context, two characteristics of any maxima of Φ are clear. First, as $(\forall\, i,j)\rho_i\rho_j|\langle\mathbf{q}_i|\mathbb{T}_{\text{opt}}|\mathbf{q}_j\rangle|^2 \geq 0$, the appearance of any cross terms ($\langle\mathbf{q}_i|\mathbb{T}_{\text{opt}}|\mathbf{q}_j\rangle$) will always decrease Φ. Therefore, to maximize Φ, a general operator $\mathbb{T}_{\text{opt}}$ must be diagonalized in the basis of $\text{Im}[\mathbb{G}^{\text{vac}}]$, Eq. (4). Second, the complex phase of $\langle\mathbf{q}_i|\mathbb{T}_{\text{opt}}|\mathbf{q}_i\rangle$ only influences the first (positive) piece of the sum, and so the value of Φ peaks when $(\forall\, i)$ $\text{atan}(\text{Im}[\langle\mathbf{q}_i|\mathbb{T}|\mathbf{q}_i\rangle]/\text{Re}[\langle\mathbf{q}_i|\mathbb{T}|\mathbf{q}_i\rangle]) = \pi/2$. Together, these two considerations show that achievable values of Φ are bounded by taking $\mathbb{T}_{\text{opt}}$ to be diagonalized by Eq. (4) with purely imaginary eigenvalues: $\mathbb{T}_{\text{opt}} = \sum_i i\tau_i|\mathbf{q}_i\rangle\langle\mathbf{q}_i|$ with $(\forall\, i)\ \tau_i \in [0, \zeta]$. As such,

$$\Phi_{\text{opt}} = \frac{2}{\pi}\sum_i \tau_i\rho_i - (\tau_i\rho_i)^2. \quad (5)$$

and maximizing the contribution of each τ_i yields

$$\Phi_{\text{opt}} = \frac{2}{\pi}\sum_i \begin{cases} 1/4 & (\zeta\rho_i \geq 1/2) \\ \zeta\rho_i - (\zeta\rho_i)^2 & \text{else.} \end{cases} \quad (6)$$

That is, based on the criterion $\zeta\rho_i \geq 1/2$, each channel in Eq. (6) produces either the Landauer limited contribution of $1/4$ [48] or the material limited $\zeta\rho_i - (\zeta\rho_i)^2$.

Interpretation.—In terms of the $\mathbb{T}$ operator, the total power extracted from any incident field $|\mathbf{E}_{\text{inc}}\rangle$ by an object is $P_{\text{ext}} = k_o\langle\mathbf{E}_{\text{inc}}|\text{Im}[\mathbb{T}]|\mathbf{E}_{\text{inc}}\rangle/(2Z)$. Comparing with Eqs. (1) and (2), Φ thus amounts to the difference of the extracted ($\text{Im}[\mathbb{T}]$) and scattered ($\mathbb{T}^\dagger\text{Im}[\mathbb{G}^{\text{vac}}]\mathbb{T}$) power for free-space states. The separation of these two forms persists throughout the derivation of the bounds, representing the linear and quadratic terms of Eq. (5). Φ_{opt} results from their connected physics.

In real space, $\text{Tr}\{\text{Im}[\mathbb{G}^{\text{vac}}]\} = \sum_i \rho_i$ is the integral of the local density of free-space states over the domain of the object. Following Eq. (6), the total power that can be extracted by an object, the first term of Eq. (2), is hence bounded by its ability to interact with radiative modes, $\text{Tr}\{\text{Im}[\mathbb{T}]\text{Im}[\mathbb{G}^{\text{vac}}]\} = \sum_i \tau_i\rho_i$, which is maximized (independently) under complete saturation of material response, $(\forall\, i)\ \tau_i = \zeta$. Relatedly, this form is also the result of applying the per-volume (shape independent) optical response limit of Ref. [35] to integrated absorption, and is similar to the light trapping bound of Ref. [34]. Because of these connections with prior work,

$$\Phi_{\text{qs}}(\omega) = \sum_i \zeta\rho_i = \zeta\int_V d\mathbf{r}\text{Im}[\mathbb{G}^{\text{vac}}(\mathbf{r}, \mathbf{r})] \quad (7)$$

serves as a useful comparison for Φ_{opt}, and is subsequently referred to as the *quasistatic bound*. This name is chosen as Eq. (7) follows from the assumption that the interaction of the object with any incident field is identically material limited, which can occur in quasistatic settings. This does *not* mean that Φ_{qs} is valid only under the quasistatic approximation. Like Φ_{opt}, Φ_{qs} is a mathematical bound derived from Maxwell's equations, although $\Phi_{\text{opt}} \leq \Phi_{\text{qs}}$ for any selection of parameters.

In Eqs. (5) and (6) this extracted power contribution is suppressed by scattering (radiative) losses, which are

captured in the quadratic term in Eq. (2) as the coupling of the polarization currents generated within an object back to free-space modes: originating through the operator $\mathbb{T}^\dagger \mathrm{Im}[\mathbb{G}^{\mathrm{vac}}]\mathbb{T}$, each τ_i represents the ability of the object to convert a given field into a current, and each radiative efficacy ρ_i the conversion of a current into outgoing radiative flux. Equivalently, the presence of strong polarization currents, necessary for strong per-volume absorption, leads to radiative losses, and these losses limit possible absorption. If $\zeta\rho_i > 1/2$, mirroring the observed dependencies of absorption ($\propto V$) and scattering ($\propto V^2$) seen in highly subwavelength metallic antennas [26,30], the growth of radiative losses with increasing τ_i can potentially surpass the growth of the extracted power, inducing saturation. As both processes are rooted in the same conversion between radiative fields and polarization currents, this critical coupling occurs at the compelling value of $\tau_i\rho_i = 1/2$ [61,62], the probability of a maximally entropic Bernoulli process, resulting in the Landauer limit value of $\Phi_{\mathrm{opt}} = 1/4$.

Analysis.—The practical usefulness of Eq. (6) stems from its favorable mathematical properties. Namely, Eq. (6) monotonically increases with ζ or any ρ_i, and, as proved in Supplemental Material [47], each ρ_i increases if the object grows (domain monotonicity). This allows us to freely decouple any true object from an imagined encompassing region of space (bounding domain). A mismatch between the domain of the object and the domain of $\mathrm{Im}[\mathbb{G}^{\mathrm{vac}}]$ must technically reduce $\|\mathbb{T}\|$ below ζ, but without any modification Eq. (6) remains an upper bound on Φ. That is, the result of Eq. (6) for any particular bounding domain is applicable to any object that can be enclosed (as well as any subdomain).

The procedure for calculating Φ_{opt} is straightforward for any bounding geometry (e.g., wires, disks, spheres, extended films, stars, disconnected patches, etc.). Precisely, the set of singular values $\{\rho_i\}$ of the domain can always be computed by forming a real-space matrix representation of $\mathrm{Im}[\mathbb{G}^{\mathrm{vac}}]$,

$$\mathrm{Im}[\mathbb{G}^{\mathrm{vac}}](\mathbf{r}) = \frac{k_o^3}{4\pi r}\left[\left(\sin(r) + \frac{\cos(r)}{r} - \frac{\sin(r)}{r^2}\right)\bar{\mathrm{I}} - \left(\sin(r) + \frac{3\ \cos(r)}{r} - \frac{3\ \sin(r)}{r^2}\right)\hat{\mathbf{r}}\otimes\hat{\mathbf{r}}\right], \tag{8}$$

with every r multiplied by a hidden k_o, and then performing a singular value decomposition of the result [49,63]. Here, to facilitate further investigation, we will focus on the high symmetry case of a ball where semianalytic evaluation is manageable (expressions for films, as well as minor additional details, are given in Supplemental Material [47]). Nevertheless, we stress that determining Φ_{opt} for domains lacking symmetry does not raise any meaningful computationally difficulties.

For this geometry two types of singular values arise:

$$\rho_\ell^{(1)} = \frac{\pi R^2}{4}\left(\frac{\ell+1}{2\ell+1}[J^2_{\ell-1/2}(R) - J_{\ell+1/2}(R)J_{\ell-3/2}(R)] + \frac{\ell}{2\ell+1}[J^2_{\ell+3/2}(R) - J_{\ell+1/2}(R)J_{\ell+5/2}(R)]\right),$$
$$\rho_\ell^{(2)} = \frac{\pi R^2}{4}[J^2_{\ell+1/2}(R) - J_{\ell-1/2}(R)J_{\ell+3/2}(R)], \tag{9}$$

where $J_\ell(-)$ is the ℓth Bessel function of the first kind with an additional factor of 2π included in its argument, each ℓ (spherical harmonic) index has a multiplicity of $(2\ell+1)$, and R is the radius of the ball normalized by the wavelength. Using standard properties of Bessel functions, it can be shown that for values of $R \gg \ell$, each of these singular values tends to the asymptote $2\pi^2 R$, and that for any combination of arguments $\rho_\ell^{(1)} < \pi(\ell+1)(\pi R)^{2\ell+1}/[2\Gamma^2(\ell+3/2)] + 2\pi\ell(\pi R)^{2\ell+5}/[(2\ell+5)(2\ell+3)\Gamma^2(\ell+5/2)]$ and $\rho_\ell^{(2)} < 2\pi(\pi R)^{2\ell+3}/[(2\ell+3)\Gamma^2(\ell+3/2)]$ (asymptotically approached for small values of R). These forms reveal two prescient general features. First, in the limit of small domains ($R \ll 1$), with "small" being determined by the value of ζ, only the first singular value of the first type contributes, and this triply degenerate (dipole) mode is responsible for the initial volume scaling necessitated by the physical meaning of the bounds. Second, the radial growth of the singular values shows that the saturation condition (impact of radiative losses) plays a major role in limiting radiative thermal emission and integrated absorption in wavelength scale volumes. [For $\zeta = 10^6$, Fig. 1(a), radiative losses lead to order-of-magnitude deviations of Φ_{opt} from Φ_{qs} beyond $R \approx 0.003\lambda$.] As visually confirmed by Fig. 1(a), as the domain grows, an increasing number of channels (multipoles) saturate, causing "steps" to appear in Φ_{opt}, and these steps lead to successively larger deviation with Φ_{qs} that ultimately regularize the initial volumetric scaling. Results for films, Fig. 1(b), are qualitatively similar. However, since the domain is infinite, the steps associated with saturation are now blended into a continuum, and the large characteristic size limit is approached from below rather than above. From a practical perspective, the fact that Φ_{opt} can achieve near ideal absorptivity for very small film thickness and moderate values of ζ is quite remarkable, a finding that is tacitly supported by a number of recent studies in 2D materials and metasurfaces [64–67]. Crucially, in either case, for any value of ζ, Φ_{opt} asymptotes to a geometric perfect absorber (the blackbody limit).

The asymptotic behavior of the singular values also reveals general characteristics of the dependence of Φ_{opt} on the material figure of merit ζ. Applying Stirling's approximation to the bounding expressions given above, for

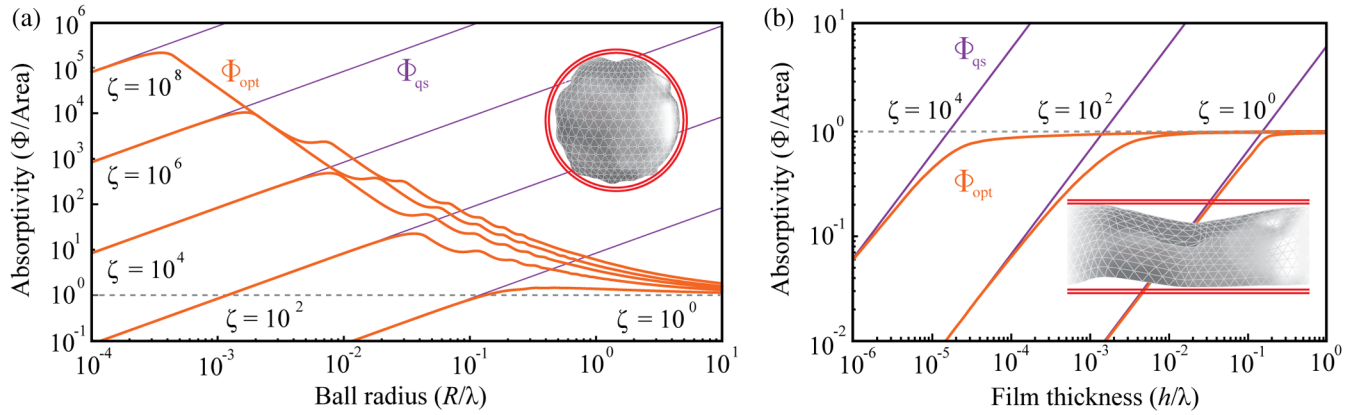

FIG. 1. Bounds on angle-integrated absorption and thermal radiation for arbitrarily structured bodies enclosed within compact and extended domains. Absorptivity (Φ normalized by area A) bounds Φ_{opt} (orange lines) and Φ_{qs} (purple lines), for a range of $\zeta = |\chi|^2/\text{Im}[\chi]$ at a fixed wavelength λ. These quantities are shown as a function of the wavelength normalized radius R of an enclosing sphere (a) and thickness h of a semi-infinite film (b). Schematics of each setting are included as insets. Even for small characteristic lengths ($\{R, h\} \leq 0.1\lambda$), Φ_{opt} is orders of magnitude smaller than Φ_{qs}.

($\ell \gg e\pi R$) we have $\rho_\ell^{(2)} \approx (e\pi R/\ell)^{2\ell+1}/4$ and $\rho_\ell^{(1)} \approx (e\pi R/\ell)^{2\ell+3}/2$, to arbitrary accuracy as ℓ becomes large. Fix R, and suppose that $\zeta = \rho_k^{(2)}$ ($\rho_k^{(1)}$ is analogous). Using the fact that $e\pi R/(k+\ell) < e\pi R/k$, the remaining (unsaturated) linear contribution of Φ_{opt} is then bounded by $9(e\pi R)^3/\{4[k^2 - (e\pi R)^2]\}$. Hence, as ζ saturates increasingly higher spherical harmonics, the contribution of the remaining unsaturated harmonics becomes increasingly small compared to the contribution of the newly saturated harmonic, $\approx(2k+1)/4$. But, saturation of the ℓth singular value (in the large ℓ limit) requires

$$\ln\left(\frac{\zeta}{2}\right) \geq (2\ell+1)\ln\left(\frac{\ell}{e\pi R}\right), \tag{10}$$

which has a sublogarithmic dependence between ℓ and ζ. Because of domain monotonicity, the above material scaling result for a ball is applicable to all compact (finite sized) objects.

This bound on material quality scaling is well matched to the features of the Φ_{opt} curves in Fig. 1(a). Once the radius has surpassed $\approx\lambda$, geometric increases in ζ ($\times 10^2$) produce relatively minute changes in the bounds. The same behavior also appears for smaller radii at larger values of ζ, but this range is not of great practical relevance since materials with ζ surpassing $\approx 10^8$ are quite rare. For instance, in the optical to infrared, $\omega \in (0.5\text{–}15)\ \mu$m, $\zeta(\omega)$ has a peak value of approximately 1.7×10^3 for gold, 2.4×10^3 for tungsten, 2.2×10^4 for silicon carbide, 6.8×10^9 for silicon, 3.3×10^7 for gallium arsenide, and 5.9×10^7 for gallium phosphide [68].

Optimizations.—Case evidence for the tightness of Eq. (6) is presented in Fig. 2. Using a gradient topology optimization algorithm [2,50], see Supplemental Material for details [47], structures nearly achieving Φ_{opt} have been discovered for two widely different domain sizes ($R = 0.05\lambda$ and $R = 0.5\lambda$) and a variety of metallic and dielectric susceptibilities. In Fig. 2, these media are grouped by imaginary susceptibility, corresponding to four different values of $\text{Im}[\chi]$, $\{0.5, 1, 2, 4\}$, with the remaining

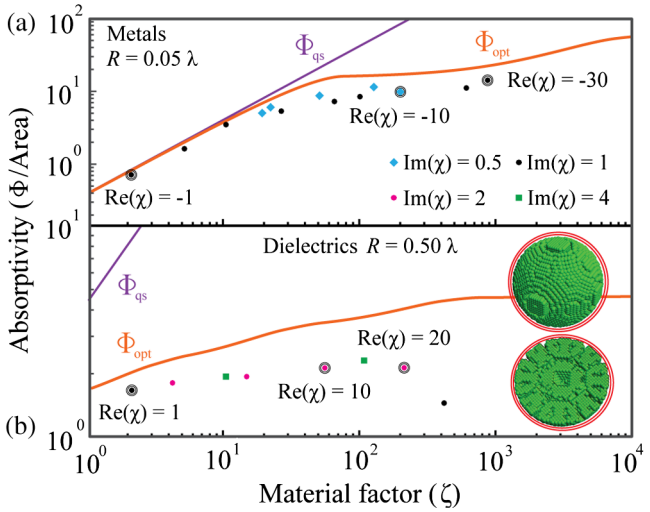

FIG. 2. Comparison of bounds with geometries discovered by inverse design. Absorptivity (Φ over area A) of structures discovered using gradient topology optimization for a variety of metallic (a) and dielectric (b) materials characterized by the material figure of merit $\zeta = |\chi|^2/\text{Im}[\chi]$. (See text for more information.) For comparison, the bounds Φ_{opt} [Eq. (6)] and Φ_{qs} [Eq. (7)] are also depicted. In (a), all structures are bound by a ball of radius $R = 0.05\lambda$. For (b), the confining domain is a ball of $R = 0.5\lambda$. The inset provides a visualization of the structure (exterior and planar cut) for the rightmost green square. The observation that optimized structures come within factors of unity of Φ_{opt} provides case evidence of the tightness of Eq. (6).

variation in ζ occurring due to $\mathrm{Re}[\chi]$. Explicit values of $\mathrm{Re}[\chi]$ are given for circled points, providing a sense of the range considered. As was previously remarked by Miller *et al.* [35], Φ_{qs} is attained for a plane wave polarized along the axis of an ellipsoidal metallic nanoparticle, given a properly chosen aspect ratio. For small values of ζ this ratio is near unity and resonant metallic structures ($\mathrm{Re}[\chi] \approx -3$) matching both bounds are easily discovered. As ζ moves to moderate values, the aspect ratio required for an ellipsoidal particle to match Φ_{qs} becomes increasingly extreme. Because of our chosen spherical boundary, discovered structures begin to deviate considerably from Φ_{qs}, but continue to come within a factor of 2 of Φ_{opt} up to $\zeta = 10^3$. Past this point, numerical issues impede our present algorithms and it remains to be seen how much of the roughly order-of-magnitude headroom allowed by Φ_{opt} is accessible.

Results for the larger domain, Fig. 2(b), show similarly good agreement. An example structure is depicted in the right-hand inset (full view and planar cut), corresponding to the rightmost green square in the plot. Comparing with the assumptions made in deriving Eq. (6), the $\mathbb{T}$ operator for this structure ($\chi = 20 + 4i$, $\Phi = 0.60\ \Phi_{\mathrm{opt}}$) is indeed found to be nearly diagonal in the basis of $\mathrm{Im}[\mathbb{G}^{\mathrm{vac}}]$ and has almost completely imaginary eigenvalues (for supporting data, see Supplemental Material [47]).

Remarks.—There are a few points that should be considered when using Eq. (6), or comparing to prior literature. First, Φ_{opt} is a bound on thermal emission and integrated absorption for a given domain and ζ factor. By choosing different geometries and material parameters, Eq. (6) can be applied to any desired context, but the confining volume is an essential feature. Second, there is no universal guarantee of tightness. Beyond the demonstrated agreement of the bounds with known quasistatic and ray optics asymptotics, the only *a priori* guarantee is domain monotonicity; there are likely volumes and material parameters where the value of Φ_{opt} will be larger than the true Φ of any practical structure. Next, while we have only considered single wavelengths, there is no reason the bounds cannot be applied to finite frequency ranges. The derivation of Φ_{opt} presented above does not incorporate any spectral sum rules (derived from causality), such as the fact that $\mathbb{T}_{\mathrm{opt}}$ should obey Kramers-Kronig dispersion relations, but for resonant absorption or thermal emission simply multiplying the bound by the width of the resonance should not produce a substantially looser bound than Φ_{opt} at the peak wavelength. (As an expedient, taking Φ_{opt} to be the peak value of a Lorentzian function of width $\Delta\omega = \omega \mathrm{Im}\chi/|\chi|$ is likely a fair approximation.) Finally, as suggested in the introduction, Φ_{opt} can be interpreted as the extension of prior multipole analysis [25–33] or communication limits [37,38], to general domains with the crucial addition that an upper bound is set on the number modes which may contribute through the pseudorank of the imaginary part of the vacuum Green function ($\mathrm{Im}[\mathbb{G}^{\mathrm{vac}}]$) and the material figure of merit (ζ), Eq. (3). We foresee this rank revealing capability potentially providing a number of benefits for future practical design and optimization. We also note that much of what has been developed in this Letter is applicable not only to generalized electromagnetic scattering (for incident plane waves or dipolar emitters with applications to solar cells, light-emitting diodes, and single-photon emitters) but also to quantum mechanics, acoustics, and other wave physics.

This work was supported by the National Science Foundation under Grants No. DMR-1454836, No. DMR 1420541, and No. DGE 1148900, the Cornell Center for Materials Research MRSEC (Grant No. DMR1719875), the Defense Advanced Research Projects Agency (DARPA) under agreement HR00111820046, and the National Science and Engineering Research Council of Canada under PDF-502958-2017. The views, opinions, and findings expressed herein are those of the authors and should not be interpreted as representing the official views or policies of any institution.

*Corresponding author.
arod@princeton.edu

[1] A. F. Koenderink, A. Alu, and A. Polman, Science **348**, 516 (2015).
[2] S. Molesky, Z. Lin, A. Y. Piggott, W. Jin, J. Vucković, and A. W. Rodriguez, Nat. Photonics **12**, 659 (2018).
[3] P. Du and J. S. Yu, Chem. Eng. J. (Lausanne) **327**, 109 (2017).
[4] J. K. Tong, W.-C. Hsu, Y. Huang, S. V. Boriskina, and G. Chen, Sci. Rep. **5**, 10661 (2015).
[5] L. Zhu, A. P. Raman, and S. Fan, Proc. Natl. Acad. Sci. U.S.A. **112**, 12282 (2015).
[6] O. Ilic, P. Bermel, G. Chen, J. D. Joannopoulos, I. Celanovic, and M. Soljačić, Nat. Nanotechnol. **11**, 320 (2016).
[7] C. F. Bohren and D. R. Huffman, *Absorption and Scattering of Light by Small Particles* (John Wiley & Sons, New York, 2008).
[8] M. I. Tribelsky, Europhys. Lett. **94**, 14004 (2011).
[9] Z. Ruan and S. Fan, Appl. Phys. Lett. **98**, 043101 (2011).
[10] S.-A. Biehs and P. Ben-Abdallah, Phys. Rev. B **93**, 165405 (2016).
[11] V. Fernández-Hurtado, A. I. Fernández-Domínguez, J. Feist, F. J. García-Vidal, and J. C. Cuevas, Phys. Rev. B **97**, 045408 (2018).
[12] D. Thompson, L. Zhu, R. Mittapally, S. Sadat, Z. Xing, P. McArdle, M. M. Qazilbash, P. Reddy, and E. Meyhofer, Nature (London) **561**, 216 (2018).
[13] M. A. Kats and F. Capasso, Laser Photonics Rev. **10**, 735 (2016).
[14] P. N. Dyachenko, S. Molesky, A. Y. Petrov, M. Störmer, T. Krekeler, S. Lang, M. Ritter, Z. Jacob, and M. Eich, Nat. Commun. **7**, 11809 (2016).
[15] S. Kruk and Y. Kivshar, ACS Photonics **4**, 2638 (2017).

[16] M. Khorasaninejad and F. Capasso, Science **358**, eaam8100 (2017).
[17] S. Hampson, W. Rowe, S. D. Christie, and M. Platt, Sens. Actuators B **256**, 1030 (2018).
[18] E. Yablonovitch, J. Opt. Soc. Am. **72**, 899 (1982).
[19] H. A. Atwater and A. Polman, Nat. Mater. **9**, 205 (2010).
[20] N. Zhang, C. Han, Y.-J. Xu, J. J. Foley IV, D. Zhang, J. Codrington, S. K. Gray, and Y. Sun, Nat. Photonics **10**, 473 (2016).
[21] D. Jariwala, A. R. Davoyan, J. Wong, and H. A. Atwater, ACS Photonics **4**, 2962 (2017).
[22] J. D. Thompson, T. Tiecke, N. P. de Leon, J. Feist, A. Akimov, M. Gullans, A. S. Zibrov, V. Vuletić, and M. D. Lukin, Science **340**, 1202 (2013).
[23] T. Galfsky, H. Krishnamoorthy, W. Newman, E. Narimanov, Z. Jacob, and V. Menon, Optica **2**, 62 (2015).
[24] N. Somaschi, V. Giesz, L. De Santis, J. Loredo, M. P. Almeida, G. Hornecker, S. L. Portalupi, T. Grange, C. Antón, J. Demory, C. Gómez, I. Sagnes, N. D. Lanzillotti-Kimura, A. Lemaítre, A. Auffeves, A. G. White, L. Lanco, and P. Senellart, Nat. Photonics **10**, 340 (2016).
[25] J. S. McLean, IEEE Trans. Antennas Propag. **44**, 672 (1996).
[26] R. E. Hamam, A. Karalis, J. D. Joannopoulos, and M. Soljačić, Phys. Rev. A **75**, 053801 (2007).
[27] D.-H. Kwon and D. M. Pozar, IEEE Trans. Antennas Propag. **57**, 3720 (2009).
[28] Z. Yu, A. Raman, and S. Fan, Proc. Natl. Acad. Sci. U.S.A. **107**, 17491 (2010).
[29] Z. Yu, A. Raman, and S. Fan, Opt. Express **18**, A366 (2010).
[30] Z. Ruan and S. Fan, Phys. Rev. Lett. **105**, 013901 (2010).
[31] J.-P. Hugonin, M. Besbes, and P. Ben-Abdallah, Phys. Rev. B **91**, 180202(R) (2015).
[32] Y. Jia, M. Qiu, H. Wu, Y. Cui, S. Fan, and Z. Ruan, Nano Lett. **15**, 5513 (2015).
[33] Y. Yang, O. D. Miller, T. Christensen, J. D. Joannopoulos, and M. Soljacic, Nano Lett. **17**, 3238 (2017).
[34] D. M. Callahan, J. N. Munday, and H. A. Atwater, Nano Lett. **12**, 214 (2012).
[35] O. D. Miller, A. G. Polimeridis, M. T. H. Reid, C. W. Hsu, B. G. DeLacy, J. D. Joannopoulos, M. Soljačić, and S. G. Johnson, Opt. Express **24**, 3329 (2016).
[36] R. Fuchs and S. Liu, Phys. Rev. B **14**, 5521 (1976).
[37] O. D. Miller, C. W. Hsu, M. T. H. Reid, W. Qiu, B. G. DeLacy, J. D. Joannopoulos, M. Soljačić, and S. G. Johnson, Phys. Rev. Lett. **112**, 123903 (2014).
[38] H. Shim, L. Fan, S. G. Johnson, and O. D. Miller, Phys. Rev. X **9**, 011043 (2019).
[39] Z. Ruan and S. Fan, Phys. Rev. A **85**, 043828 (2012).
[40] F. Alpeggiani, N. Parappurath, E. Verhagen, and L. Kuipers, Phys. Rev. X **7**, 021035 (2017).
[41] D. A. B. Miller, Appl. Opt. **39**, 1681 (2000).
[42] D. A. B. Miller, J. Opt. Soc. Am. B **24**, A1 (2007).
[43] C. Sohl, M. Gustafsson, and G. Kristensson, J. Phys. D **40**, 7146 (2007).
[44] M. Gustafsson, C. Sohl, and G. Kristensson, Proc. R. Soc. A **463**, 2589 (2007).
[45] M. Krüger, G. Bimonte, T. Emig, and M. Kardar, Phys. Rev. B **86**, 115423 (2012).
[46] J.-J. Greffet and M. Nieto-Vesperinas, J. Opt. Soc. Am. A **15**, 2735 (1998).
[47] See Supplemental Material at http://link.aps.org/supplemental/10.1103/PhysRevLett.123.257401, which includes Refs. [2,45,48–60], for a brief review of scattering theory, the inverse design method employed and mathematical support of the film results.
[48] S. Molesky, P. S. Venkataram, W. Jin, and A. W. Rodriguez, arXiv:1907.03000 [Phys. Rev. B (to be published)].
[49] A. G. Polimeridis, M. T. H. Reid, W. Jin, S. G. Johnson, J. K. White, and A. W. Rodriguez, Phys. Rev. B **92**, 134202 (2015).
[50] J. S. Jensen and O. Sigmund, Laser Photonics Rev. **5**, 308 (2011).
[51] B. A. Lippmann and J. Schwinger, Phys. Rev. **79**, 469 (1950).
[52] W. Jin, S. Molesky, Z. Lin, and A. W. Rodriguez, Phys. Rev. B **99**, 041403(R) (2019).
[53] W. Eckhardt, Physica (Amsterdam) **128A**, 467 (1984).
[54] L. Tsang, J. A. Kong, and K.-H. Ding, *Scattering of Electromagnetic Waves: Theories and Applications* (John Wiley & Sons, New York, 2004), Vol. 27.
[55] K. Svanberg, SIAM J. Opt. **12**, 555 (2002).
[56] S. G. Johnson, https://nlopt.readthedocs.io/en/latest/.
[57] W. Jin, A. G. Polimeridis, and A. W. Rodriguez, Phys. Rev. B **93**, 121403(R) (2016).
[58] A. Hochman, J. Fernandez Villena, A. G. Polimeridis, L. M. Silveira, J. K. White, and L. Daniel, IEEE Trans. Antennas Propag. **62**, 3150 (2014).
[59] N. Halko, P.-G. Martinsson, and J. A. Tropp, SIAM Rev. **53**, 217 (2011).
[60] P.-G. Martinsson, V. Rokhlin, and M. Tygert, Appl. Comput. Harmon. Anal. **30**, 47 (2011).
[61] J. Pendry, J. Phys. A **16**, 2161 (1983).
[62] J. Pendry, J. Phys. Condens. Matter **11**, 6621 (1999).
[63] A. G. Polimeridis, F. Vipiana, J. R. Mosig, and D. R. Wilton, IEEE Trans. Antennas Propag. **61**, 3112 (2013).
[64] S. Thongrattanasiri, F. H. Koppens, and F. J. G. De Abajo, Phys. Rev. Lett. **108**, 047401 (2012).
[65] G. M. Akselrod, J. Huang, T. B. Hoang, P. T. Bowen, L. Su, D. R. Smith, and M. H. Mikkelsen, Adv. Mater. **27**, 8028 (2015).
[66] S. Kim, M. S. Jang, V. W. Brar, K. W. Mauser, L. Kim, and H. A. Atwater, Nano Lett. **18**, 971 (2018).
[67] J. Nong, H. Da, Q. Fang, Y. Yu, and X. Yan, J. Phys. D **51**, 375105 (2018).
[68] E. D. Palik, *Handbook of Optical Constants of Solids* (Academic Press, New York, 1998), Vol. 3.